Research Paper

Timing of carbonatite-hosted U-polymetallic mineralization in the supergiant Huayangchuan deposit, Qinling Orogen: Constraints from titanite U–Pb and molybdenite Re–Os dating

Hui Zheng [a,b], Huayong Chen [a,*], Dengfeng Li [c], Chao Wu [a,b], Xi Chen [d], Chun-kit Lai [e]

[a] Key Laboratory of Mineralogy and Metallogeny, Guangzhou Institute of Geochemistry, Chinese Academy of Sciences, Guangzhou 510640, China
[b] University of Chinese Academy of Sciences, Beijing 100049, China
[c] School of Marine Sciences, Sun Yat-sen University, Guangzhou 510006, China
[d] School of Earth Science and Technology, Southwest Petroleum University, Chengdu 610000, China
[e] Faculty of Science, Universiti Brunei Darussalam, Gadong, BE1410, Brunei Darussalam

ABSTRACT

The newly-discovered supergiant Huayangchuan uranium (U)-polymetallic (Sr, Se, REEs, Ba, Nb and Pb) deposit is located in the Qinling Orogen, central China. The deposit underwent multistage mineralization, with the main carbonatite ore stage being the most important for the U, Nb, REE, Sr and Ba endowments. According to the mineral assemblages, the main carbonatite ore stage can be divided into three substages, i.e., sulfate (Ba–Sr), alkali-rich U and REE-U mineralization.

Main-stage titanite from the Huayangchuan igneous carbonatite are rich in high field strength elements (HFSEs, e.g., Zr, Nb and REEs), and show clear elemental substitutions (e.g., Ti vs. Nb + Fe + Al and Ca + Ti vs. Fe + Al + REE). High-precision LA-ICP-MS titanite dating yielded a U–Pb age of 209.0 ± 2.9 Ma, which represents the main-stage mineralization age at Huayangchuan, and is coeval with the local carbonatite dyke intrusion. This mineralization age is further constrained by the Re–Os dating of molybdenite from the Huayangchuan carbonatite, which yielded a weighted mean age of 196.8 ± 2.4 Ma. Molybdenite Re contents (337.55–392.75 ppm) and C-O-Sr-Nd-Pb isotopic evidence of the Huayangchuan carbonatite both suggest a mantle origin for the carbonatite. Our study supports that the Late Triassic carbonatite magmatism was responsible for the world-class U-Mo-REE mineralization in the Qinling Orogen, and that the regional magmatism and ore formation was likely caused by the closure of the Mianlue ocean and the subsequent North China-South China continent-continent collision.

1. Introduction

Carbonatite is a special and uncommon rock type in the world, and many studies were dedicated to unravel its origin, genesis, classification, distribution and mineralization (Taylor et al., 1967; Le Bas, 1981; Nelson et al., 1988; Le Bas et al., 1992; Sweeney, 1994; Woolley and Kjarsgaard, 2008; Jones et al., 2013; Simandl and Paradis, 2018). Carbonatites are associated with diverse mineral resources, e.g., REE, Ba, Sr, Nb, Ta, Cu, Ti, U, Th, Zr, Fe, V, Au, F and P (Woolley and Kjarsgaard, 2008; Simandl and Paradis, 2018). Famous carbonatite-hosted deposits include the Bayan Obo REE deposit (northern China), Mountain Pass REE deposit (California, USA) and Araxa Nb deposit (Brazil). Woolley and Kjarsgaard (2008) estimated a total number of 527 carbonatite occurrences in the world, among which only 112 contain economic mineralization. Only a few carbonatite-type uranium (U)-bearing deposits were discovered, including the Phalaborwa and Sankopsdrif deposits (South Africa), and the Manitou Islands deposit (Ontaria, Canada) (Dahlkamp, 1993; Woolley and Kjarsgaard, 2008), and most of them only contain sub-economic U mineralization. In recent ten years, the supergiant Huayangchuan carbonatite-hosted U-polymetallic deposit was discovered in the Qinling Orogen (central China), which is characterized by dominant U with abundant Sr, Nb, Ba, REE, Pb, Ag and Bi resources (Gao et al., 2017; He et al., 2018; Kang et al., 2018).

Many studies have been published on the carbonatites at Huayangchuan, including their petrography and geochemistry, which all pointed to an igneous origin (Yu, 1992; Xu et al., 2007; Wang et al., 2011; Reguir

et al., 2012; Hui and He, 2016; Song et al., 2016; Hui et al., 2017). Huayangchuan deposit developed multistage mineralization, and the main ore stage at Huayangchuan is associated with the carbonatites, with the majority of U and REE (and all Ba, Sr and Nb) mineralization hosted in carbonatite or fenite (metasomatic altered carbonatite) dykes. Yu (1992) first reported a phlogopite K–Ar age of 181 Ma for the Huayangchuan carbonatite, and then Indosinian K–Ar ages of 206–204 Ma on fresh feldspar and whole-rock carbonatite were also reported by the same research group (Qiu et al., 1993). More recently, He et al. (2016) obtained a Cretaceous biotite (in carbonatite) Ar–Ar age of 132.58 ± 0.70 Ma. Therefore, the actual timing of carbonatite magmatism and its related main-stage mineralization at Huayangchuan is still uncertain.

Titanite (or sphene, with the ideal formula $CaTiOSiO_4$) is a common accessory mineral that coexists with the main U-bearing mineral (i.e., pyrochlore (UO_2: 26.28–33.56 wt.%)) at Huayangchuan. Because of its high closure temperature (>700 °C; Cherniak, 1993; Frost et al., 2000; Aleinikoff et al., 2002) and its U-bearing nature (Kohn, 2017), U–Pb dating of titanite has been successively applied to many igneous and metamorphosed rocks in recent years (Aleinikoff et al., 2002; Storey

et al., 2006; Gao et al., 2012; Morley and Arboit, 2019). Titanite U–Pb dating is also applied to constrain mineralization ages, e.g., IOCG deposits in Kiruna District (Sweden) (Smith et al., 2009), and polymetallic skarn deposits at Tonglushan (Li et al., 2010), Jinshandian (Zhu et al., 2014), Beiya (Fu et al., 2016), Zhuxi (Song et al., 2019) and Pingbao (Li et al., 2019) in China. In this study, we chose the main ore (carbonatite) stage titanite for U–Pb dating, and REE-U ore-related molybdenite in carbonatite for Re–Os dating to constrain the timing of mineralization at Huayangchuan. We discuss the relationship between the Huayangchuan ore formation and the Triassic evolution of the Qinling Orogen.

2. Regional and deposit geology

The Huayangchuan U-polymetallic deposit is located in Shaanxi Province, central China, and geologically located in the northern Qinling Orogen (Fig. 1A). From south to north, the orogen is divided into: (1) northern margin of Yangtze Block, (2) South Qinling, (3) North Qinling and (4) southern margin of North China Block (where Huayangchuan is located), along the Mianlue, Shangnan-Danfeng and Luanchuan faults, respectively (Fig. 1B). Apart from Huayangchuan, the Qinling Orogen
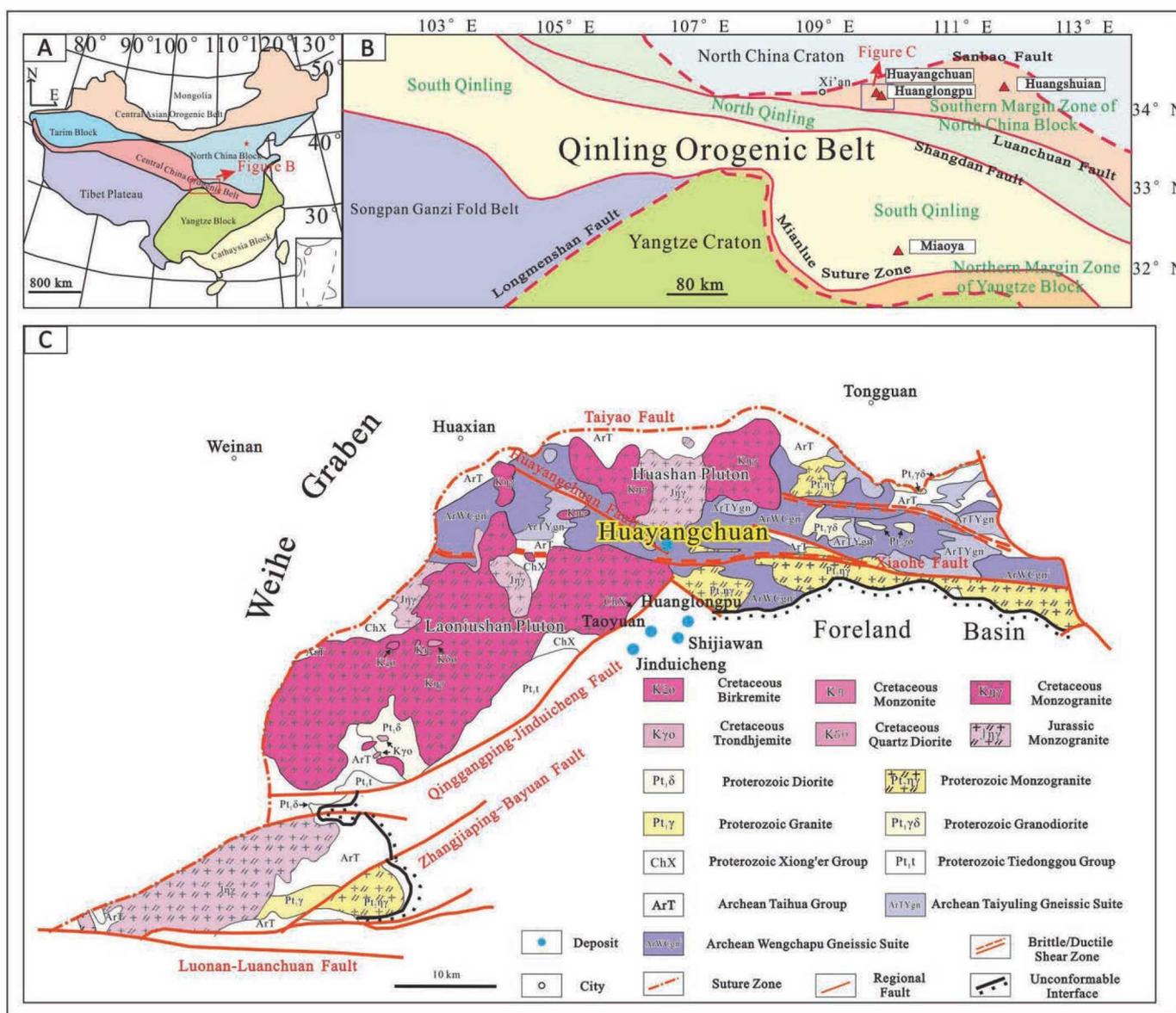

Fig. 1. (A) Geologic sketch map of China. (B) Regional tectonic map of Qinling Orogen. (C) Geologic map of the Huayangchuan district (modified after Gao et al., 2017).

also contains other carbonatite-hosted deposits, including the Huanglongpu Mo-Pb(-Re), Huangshuian Mo and Miaoya REE deposits (Fig. 1B; Huang et al., 1985, 1994, 2009; Xu et al., 2007, 2008). According to division of East Qinling and West Qinling by Laoniushan Complex (Li et al., 2004), Huayangchuan deposit should belong to East Qinling.

Local stratigraphic units at Huayangchuan comprise the Archean Taihua Group, and the Proterozoic Xiong'er and Tiedonggou groups, all of which are high-grade metamorphosed. Biotite-plagioclase-(amphibole) gneiss of the Taihua Group is the main outcropping sequence at Huayangchuan. Metamorphic core complex, folds and faults extensively developed in the region. Major faults (e.g., Taiyao, Xiaohe, Huayangchuan, Luonan-Luanchuan; Fig. 1C) are all WNW- or EW-trending, superimposed by NE-trending secondary faults and fractures. The WNW-trending Huayangchuan Fault controls the major distribution of orebodies at Huayangchuan. Intrusive rocks are extensively distributed in the southern margin of North China Block, including the Archean TTG (tonalite-trondhjemite-granodiorite) gneissic suite (e.g., at Taiyuling and Wengchapu), Proterozoic granitoids (mainly diorite, granodiorite, monzogranite and granite), Jurassic monzogranite and Cretaceous granitoids (mainly quartz diorite, monzonite and monzogranite) (Fig. 1C). At Huayangchuan, magmatic rocks comprise mainly Proterozoic granite porphyry and pegmatite, Triassic carbonatite dikes, and Jurassic–Cretaceous granitoids (Fig. 2A). Apart from Huayangchuan, the district also contains other large-size deposits, e.g., the Jinduicheng and Shijiawan porphyry Mo deposits, and the Huanglongpu carbonatite-related Mo-Pb(-Re) deposit (Fig. 1C; Nie, 1994; Jiao et al., 2010).

3. Alteration and mineralization features of Huayangchuan deposit

Mineralization at Huayangchuan commonly occurs as lenses or veins, and contains over 40 common minerals, including pyrochlore, barite-celestite, monazite, allanite, galena, uranothorite and uraninite. Gangue minerals include mainly calcite, aegirine-augite, titanite, apatite, phlogopite, amphibole, biotite and garnet. Potassic alteration and fenitization are two major ore-related alteration styles. The mineral resources (e.g., U, Nb, REE, Ba and Sr) are mostly associated with or hosted in carbonatite dikes.

The mineralization usually presents as dissemination in carbonatites or contact zone between carbonatite dikes and wall rocks (Fig. 3A–F). Pyrochlore, the main U ore mineral at Huayangchuan, is usually intergrown with calcite, apatite, monazite, titanite, allanite and phlogopite. According to the mineral assemblage and paragenetic sequence, the carbonatite mineralization can be divided into three substages, i.e.,

sulfate (Ba–Sr), alkali-rich U, and REE-U mineralization. Sulfate assemblages (barite-celestite + calcite + phlogopite + yellowish barite-celestite) commonly occur as aggregates (Fig. 3A and B). The alkali-rich U assemblage contains pyrochlore (red coarse-grained euhedral) + calcite + aegirine-augite + titanite + apatite ± quartz ± magnetite ± microcline ± amphibole ± (galena + pyrite) (Fig. 3C and D). REE-U mineral assemblage contains pyrochlore (medium-fine grained) + calcite + monazite + allanite + phlogopite ± biotite ± molybdenite, and commonly occurs as crumb or aggregates (Fig. 3E and F).

4. Samples and analytical methods

4.1. Sampling and petrography

4.1.1. Titanite

Titanite is commonly found in both wall rocks (Fig. 4A) and carbonatites (Fig. 4B) at Huayangchuan. Titanite grains in the wall rocks are usually medium-coarse grained subhedral to anhedral, and coexist with biotite and contain ilmenite inclusions. In contrast, titanite grains in the carbonatites are predominately coarse-grained (0.01–1 cm) euhedral to subhedral. These titanite grains are locally of envelope-shaped with brown-reddish pleochroism, and coexist with calcite, pyrochlore, aegirine-augite, galena and apatite (Fig. 4C–E). In the alkali-rich U mineral assemblage of carbonatite, titanite usually intergrows with pyrochlore (Fig. 4E–H), suggesting that the former is syn-U mineralization. The drill core sample (ZK-2404-66, Fig. 4E) was collected at a depth of 1032.4 m (Fig. 2A, B), the titanite of this sample coexists with pyrochlore, aegirine-augite, calcite and galena, which is a typical alkali-rich mineral assemblage in Huayangchuan. Titanite grains were separated from this sample for laser ablation inductively coupled plasma mass spectrometry (LA-ICP-MS) U–Pb dating.

4.1.2. Molybdenite

Main-stage molybdenite is lead gray and fine-grained, and commonly occurs as disseminations in the carbonatites (Fig. 5A, B). Under the microscope, molybdenite usually occurs as dendritic grains or clusters associated with calcite aggregates (Fig. 5C–F), and locally intergrows with phlogopite and pyrochlore (Fig. 5C). This indicates that the molybdenite is syn-U mineralization. Four molybdenite samples in carbonatite were collected from drill core samples of ZK-2403-1 (1300.20 m depth), ZK-2403-3 (1298.22 m depth), ZK-701-6 (1349.47 m depth) and ZK-701-7 (1340.50 m depth) (Fig. 2A, B). Molybdenite separates were picked up under the microscope to achieve >99% purity for the Re–Os dating.
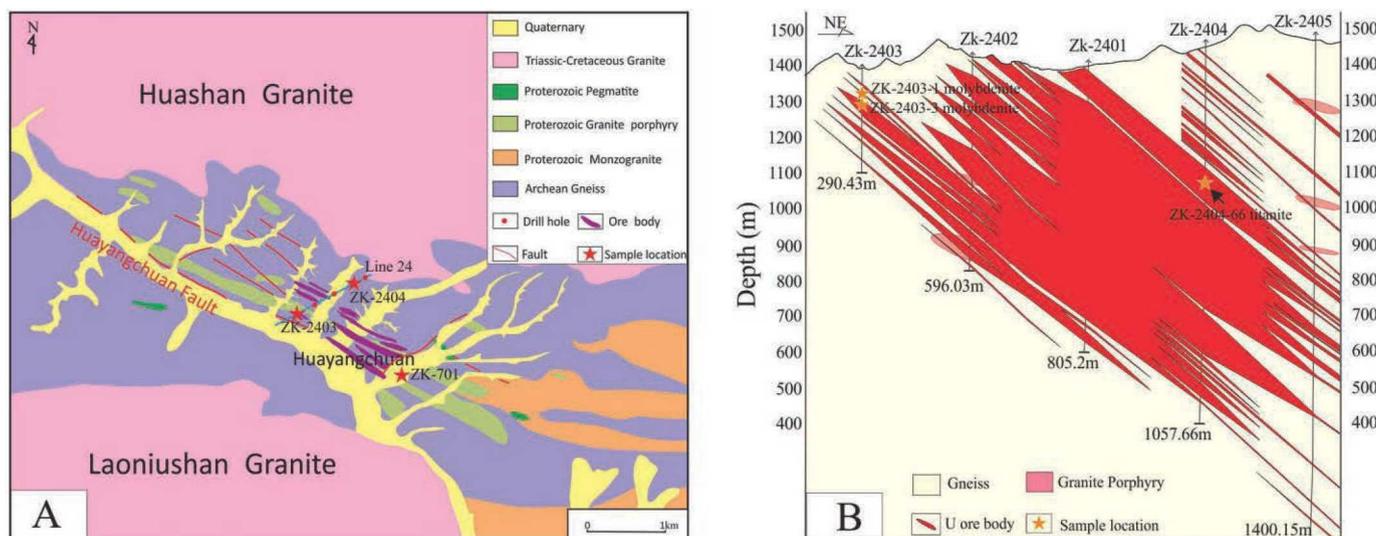

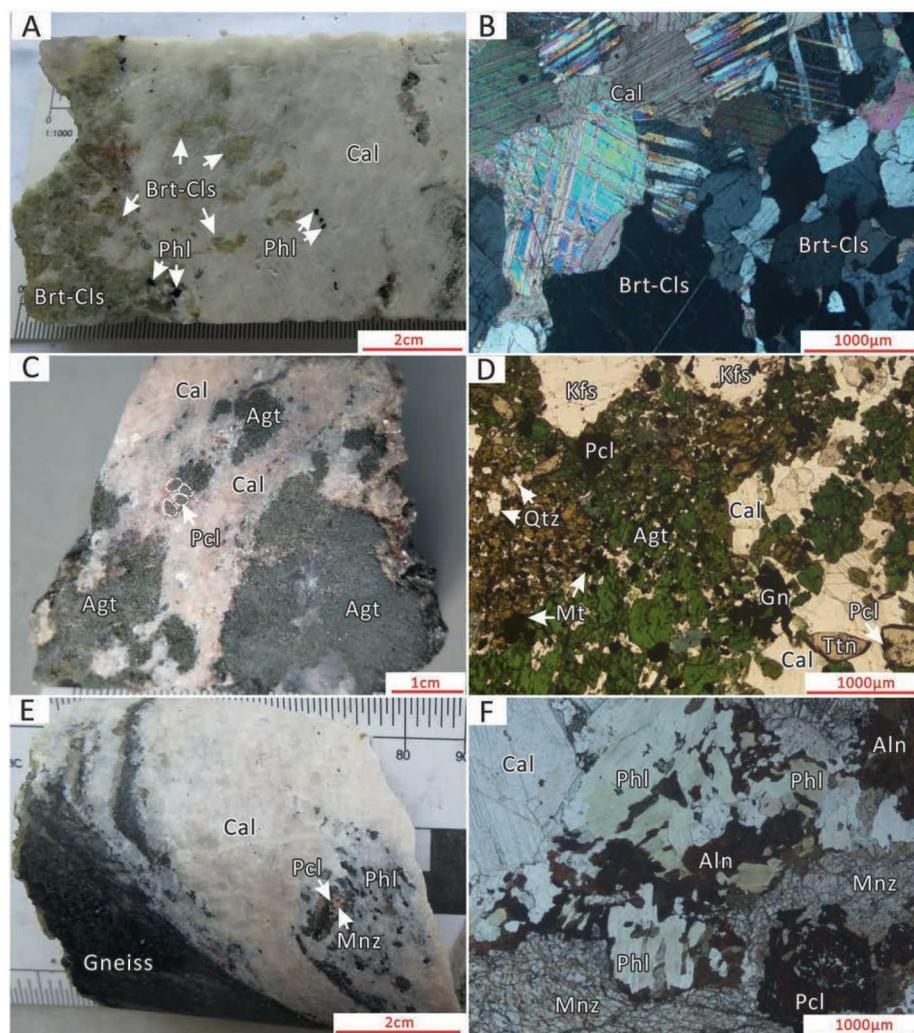Fig. 2. Simplified geologic map of the Huayangchuan deposit.

Fig. 3. Representative ore photos and photomicrographs from the Huayangchuan deposit. (A, B) Anhedral barite-celestite aggregates coexist with calcite and phlogopite. (C, D) Coarse-grained euhedral red pyrochlore intergrown with aegirine-augite, titanite, calcite and minor galena. Aegirine-augite commonly replaced by quartz. (E, F) Red subhedral medium-fine grained pyrochlore with monazite aggregates. Allanite and phlogopite commonly occur as crumby disseminations in carbonatite. Abbreviations: Aln = allanite, Kfs = K-feldspar, Brt = barite, Cls = celestite, Cal = calcite, Phl = phlogopite, Agt = aegirine-augite, Pcl = pyrochlore, Ttn = titanite, Mnz = monazite, Gn = galena, Mt = magnetite, Qtz = quartz.

4.2. Titanite EPMA and LA-ICP-MS analyses

Major elements of titanite were analyzed with a JXA-JEOL-8230 Electron Probe Microanalyzer (EPMA) at the Key Laboratory of Mineralogy and Metallogeny, Guangzhou Institute of Geochemistry, Chinese Academy of Sciences (GIGCAS). Analytical conditions include 15 kV accelerating voltage, 20 nA beam current and 1 μm beam diameter. The calibration minerals, peak time (s) and background (s) of each element are: F (BaF_2, 10, 5), Cl (Tugtupite, 10, 5), K (Orthoclase, 10, 5), Na (Albite, 10, 5), Si (Kaersutite, 20, 10), Ca (Diopside, 20, 10), Al (Kaersutite, 20, 10), Mn (Rhodonite, 40, 20), Ti (Rutile, 40, 20), Fe (Magnetite, 20, 10), Mg (Kaersutite, 20, 10), Ce (Monazite, 90, 45), Nd (Monazite, 90, 45), Nb (metal Nb, 90, 45). All data were corrected by the ZAF correction method.

The titanite separates were mounted in epoxy resin, and the subsequent titanite LA-ICP-MS U–Pb dating and trace element analysis were conducted at the Key Laboratory of Marine Resources and Coastal Engineering, Sun Yat-sen University. The analysis was conducted with a 193 nm ArF excimer laser ablation system (GeoLasPro), coupled with an Agilent 7700 × ICP-MS. Analytical conditions include 32 μm spot size, 5 J/cm^2 energy density and 5 Hz repetition rate. For sample ZK-2404-66, the isotopes analyzed include ^{51}V, ^{88}Sr, ^{89}Y, ^{93}Nb, ^{139}La, ^{140}Ce, ^{141}Pr, ^{143}Nd, ^{147}Sm, ^{151}Eu, ^{157}Gd, ^{159}Tb, ^{163}Dy, ^{165}Ho, ^{166}Er, ^{169}Tm, ^{173}Yb, ^{175}Lu, ^{90}Zr, ^{95}Mo, ^{178}Hf, ^{181}Ta, ^{232}Th, ^{204}Pb, ^{206}Pb, ^{207}Pb, ^{208}Pb, ^{238}U. The standard NIST SRM 610 was used to calibrate the trace element compositions of titanite and to correct for instrument drift, using ^{43}Ca

determined the EPMA-measured CaO concentration as the internal standard. The matrix-matching external titanite standard (OLT-1) was used to correct for U–Pb fractionation and instrumental mass discrimination. One NIST SRM 610 and two OLT-1 titanite standard were analyzed for every 10 samples. Each analysis consists of a 18 s background measurement (laser-off) followed by 45 s sample data acquisition. Offline data reduction was performed using ICPMSDataCal software (Liu et al., 2010). Meanwhile, IsoplotR online was used to construct the Tera–Wasserburg diagram (Vermeesch, 2018). In this study, analysis of the OLT-1 titanite yielded ^{206}Pb/^{238}U ages of 1002–1025 Ma ($n = 12$), consistent (within error) with the reported ID-TIMS age of 1014.8 ± 2.0 Ma (2σ, MSWD = 1.8) (Kenedy et al., 2010).

4.3. Titanite U–Pb dating

For U–Pb dating of many minerals (e.g., zircon, titanite, apatite, allanite, garnet and rutile), incorporation of non-radiogenic common Pb (Pb_C) is non-negligible (Andersen, 2002; Chew et al., 2014; Fu et al., 2016; Scibiorski et al., 2019). Thus, the choice of common Pb composition would significantly affect the calculated ages, especially for young (post-Paleozoic) samples (Frost et al., 2000). The initial Pb can be determined by analyzing the Pb component of coexisting non-U-bearing minerals, such as pyrite, galena or K-feldspar (Frost et al., 2000; Andersen, 2002; Chew et al., 2014; Li et al., 2019). The application of ^{204}Pb-correction can be affected by the Ar nebulizer gas used in LA-ICP-MS, and is thus infeasible for titanite Pb-correction (Andersen,
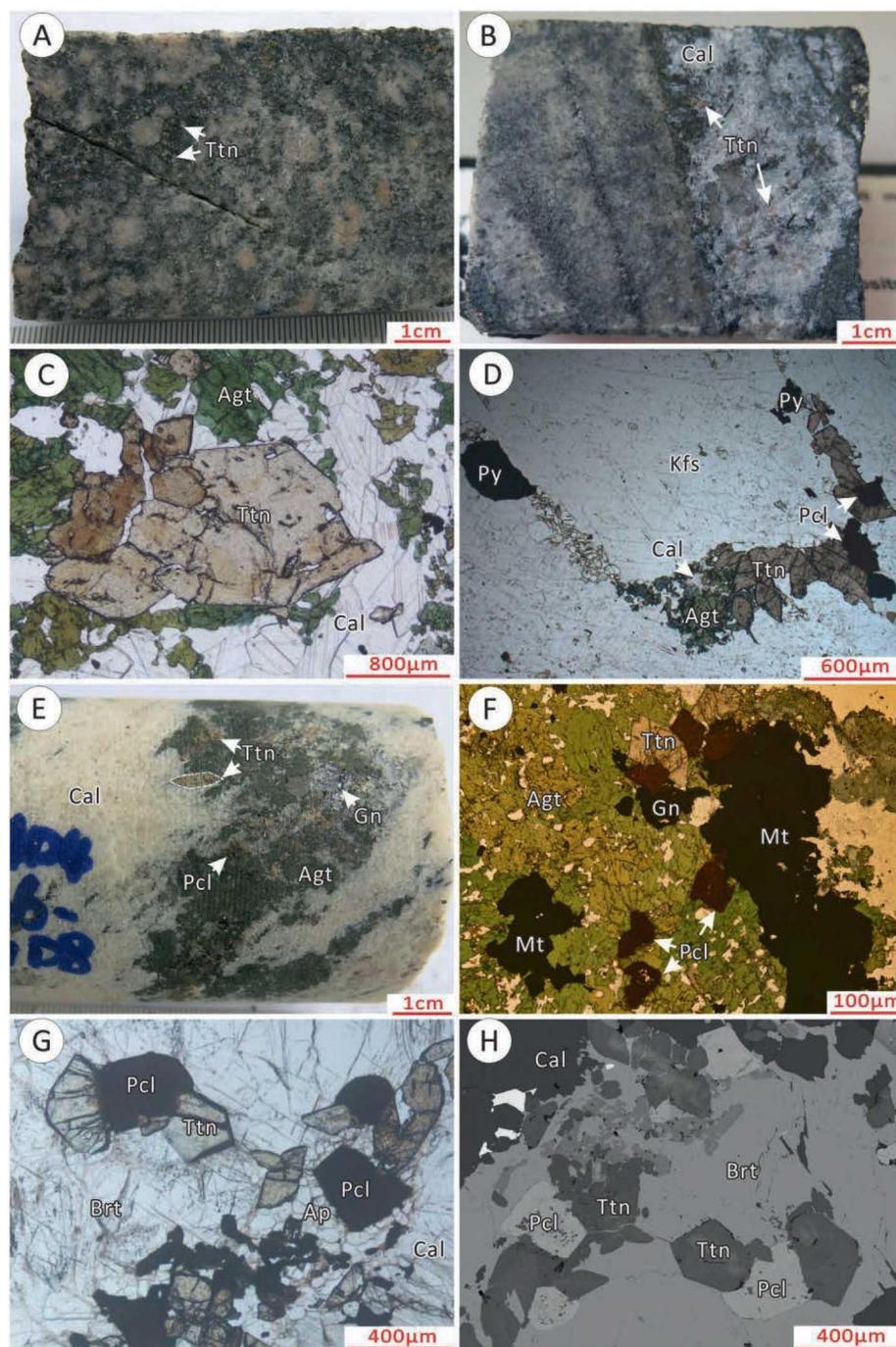
Fig. 4. Photos and microphotographs of typical titanite in the Huayangchuan deposit. (A) Fine-grained titanite in wall rock. (B) Coarse-grained sub-hedral-euhedral titanite in carbonatite. (C) Coarse-grained subhedral-euhedral titanite in carbonatite, showing clear red-brown pleochroism under the microscope. (D) Vein (pyrochlore-titanite-calcite-aegirine-augite-pyrite) crosscut wall rock. (E) Alkaline-rich U assemblage in carbonatite (pyrochlore + titanite + calcite + aegirine-augite + galena) in hand specimen, titanite shows coarse-grained euhedral diamond-shaped. (F) Alkaline-rich U assemblage (aegirine-augite + titanite + pyrochlore + magnetite + galena) under the microscope. (G–H) Pyrochlore coexists with titanite. Abbreviations: Ttn = titanite, Cal = calcite, Agt = aegirine-augite, Kfs = K-feldspar, Pcl = pyrochlore, Brt = barite, Ap = apatite, Py = pyrite, Gn = galena, Mt = magnetite.

2002; Scibiorski et al., 2019). ^{208}Pb-correction is mainly applied to low Th/U (<0.5) without Th-bearing minerals (Zack et al., 2011; Chew et al., 2014). At present, ^{207}Pb-correction methods for Pb$_C$ of the titanite has been widely used (Simonetti et al., 2006; Storey et al., 2006; Fu et al., 2016; Li et al., 2019; Scibiorski et al., 2019; Song et al., 2019). Recent investigation showed that selection of appropriate common Pb for titanite is crucial (Kirkland et al., 2018). However, there are very few appropriate data of non-U-bearing minerals that coexist with titanite at Huayangchuan. Furthermore, using model Pb isotope (Stacey and Kramers, 1975) is not appropriate with high common Pb (common ^{206}Pb > 10%) (Aleinikoff et al., 2002; Fu et al., 2016). Thus, the lower intercept age can better stand for titanite U–Pb dating, rather than ^{207}Pb-correction age using y-intercept as initial ^{207}Pb/^{206}Pb (Lorie et al., 2019). Therefore, the uncorrected data were plotted in the Tera-Wasserburg (^{238}U/^{206}Pb –

^{207}Pb/^{206}Pb) diagram (Vermeesch, 2018), yielding a lower intercept and y-intercept of the regression.

4.4. Molybdenite Re–Os dating

Molybdenite Re–Os dissolution, preparation and isotopic analysis were performed at the Key Laboratory of Isotope Geochronology and Geochemistry (GIGCAS). Molybdenite Re–Os isotope preliminary treatment was done with the Carius tube method. ^{185}Re spike was added to each fine-grained molybdenite sample (0.0136–0.0239 g), and normal Os standard solutions and 10 mL concentrated HNO$_3$ were digested in the Carius tube. Meanwhile, the lower part of the tube was immersed in an ethanol-liquid nitrogen slush. The tube was then sealed and heated at 225–230 °C for 24 h. After the sample digestion, the tube was refrozen
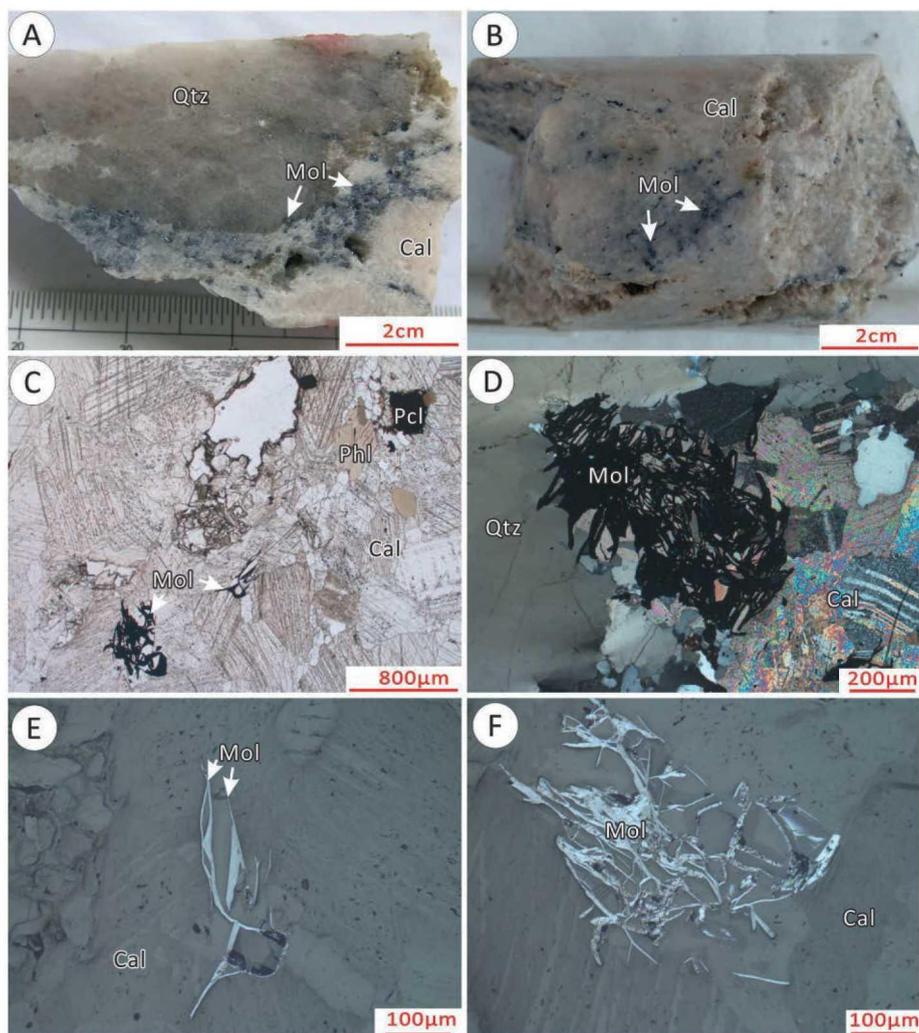
Fig. 5. Photos and microphotographs of typical molybdenite in the Huayangchuan deposit. (A, B) Disseminated molybdenite in carbonatite. (C–F) Dendritic/flaky molybdenite intergrown with calcite, phlogopite and pyrochlore in the carbonatite. Abbreviations: Mol = molybdenite, Cal = calcite, Phl = phlogopite, Pcl = pyrochlore, Qtz = quartz.

and then opened. Subsequently, an approximate amount of supernatant was transferred to a 30 mL quartz beaker from the opened tube, dried by heating at 150 °C, and then added of 0.5 mL concentrated HNO_3 and dried-down. This step was repeated twice to ensure the removal of Os as OsO_4, and finally diluted to a 10 mL 2% HNO_3 for the Re measurement by a X series II quadrupole ICP-MS (Thermo Fisher Scientific) (Sun et al., 2001, 2010; Li et al., 2011; Wang et al., 2018). The remaining supernatant was directly poured into a 50 mL distillation flask redesigned after Sun et al. (2001, 2010), and distilled at 110 °C for 20 min, and trapped using 5 mL H_2O chilled in a water-ice bath for Os extraction.

5. Results

5.1. Major and trace elements of titanite

Major element data of titanite from the Huayangchuan carbonatite are presented in Supplementary Table 1. The titanite has SiO_2 of 28.64–30.36 wt.%, TiO_2 of 29.82–36.43 wt.%, CaO of 25.19–28.41 wt.%, Nb_2O_5 of 0.58–4.38 wt.%, F of 0.07–0.56 wt.%, FeO of 1.88–3.77 wt.%, Al_2O_3 of 0.21–2.54 wt.%, Ce_2O_3 of 0–0.99 wt.% and Nd_2O_3 of 0.11–1.07 wt.%, with minor Na_2O (0–0.53 wt.%), MgO (0.02–0.70 wt.%) and MnO (0.07–0.25 wt.%). Titanite stoichiometries were calculated basing on the five equivalent oxygen atoms per formula unit (a.p.f.u). Experiment by King et al. (2013) indicated that Fe^{2+} is only minor

compared to Fe^{3+} in titanite (ca. 14%), thus all iron was regarded as Fe^{3+} for the a.p.f.u calculation (Song et al., 2019).

Trace element compositions of titanite from the Huayangchuan carbonatite are presented in Supplementary Table 2. The titanite shows high HFSE (high field strength elements) contents, such as the very high Nb (9564.67–41188.47 ppm; avg. 18043.46 ppm) that matches with the EPMA results, together with 156.28–3841.12 ppm Zr (avg. 961.41 ppm), 0.17–2.01 ppm Mo (avg. 0.99 ppm), 7.41–22.77 ppm Lu (avg. 12.10 ppm), 4.01–192.63 ppm Hf (avg. 37.20 ppm), 1.29–40.19 ppm Ta (avg. 10.44 ppm), 34.08–757.26 ppm U (avg. 116.80 ppm), 31.46–192.57 ppm Th (avg. 67.02 ppm), 1308.51–3203.22 ppm V (avg. 2090.54 ppm), 437.26–734.54 ppm Sr (avg. 550.20 ppm). Th/U, Nb/Ta and Lu/Hf ratios are 0.17–3.08 (avg. 0.74), 546.62–16958.10 (avg. 3012.02) and 0.07–3.43 (avg. 0.97), respectively. Titanite also contains very high ΣREY (total rare earth elements plus Y contents) of 17478.26–32781.10 ppm (avg. 25379.52 ppm), among which ΣLREE are 14271.13–27425.81 ppm (avg. 20685.27 ppm) and HREE are 1729.37–3328.04 ppm (avg. 2397.75 ppm). The LREE/HREE ratio ranges between 6.09 and 11.39 (avg. 8.71), showing a LREE/HREE–enriched pattern. The range of $(La/Sm)_{CN}$ (chondrite normalized), $(La/Yb)_N$ and $(Sm/Yb)_N$ are 0.44–0.86 (avg. 0.61), 4.00–14.33 (avg. 8.50) and 8.39–19.87 (avg. 13.83), respectively, with no apparent Eu anomalies (δEu: 0.94–1.06, avg. 0.99) and weakly positive Ce anomalies (δCe: 1.22–1.31, avg. 1.27).

5.2. Titanite U–Pb age

The measured U/Pb ratios of titanite are presented in Table 1. The uncorrected data are plotted in the Tera-Wasserbury diagram. The common Pb-corrected data of the Huayangchuan titanite define a linear array, yielding a lower intercept crystallization age of 209.0 ± 2.9 Ma (Fig. 6; MSWD = 2.1; n = 43).

5.3. Molybdenite Re–Os age

Re–Os isotopic data for the four Huayangchuan molybdenite samples are presented in Table 2. All Re concentrations are high (337.55–392.75 ppm). The ^{187}Os contents and model ages are of 768.34–816.99 ppb and 195.40–198.33 Ma (avg. 196.8 ± 2.4 Ma, MSWD = 2.3), respectively. The ^{187}Re-^{187}Os isochron age of 206 ± 59 Ma (MSWD = 2.9) was obtained by ISOPLOT program (Ludwig, 2003), with initial ^{187}Os value of −0.04 ± 0.23 ppm (Fig. 7A–B). The ^{187}Os interception is near zero with error. Implying that the molybdenite contains little or no non-radiogenic ^{187}Os, which indicates that the weighted mean age is reliable (Leng et al., 2012).
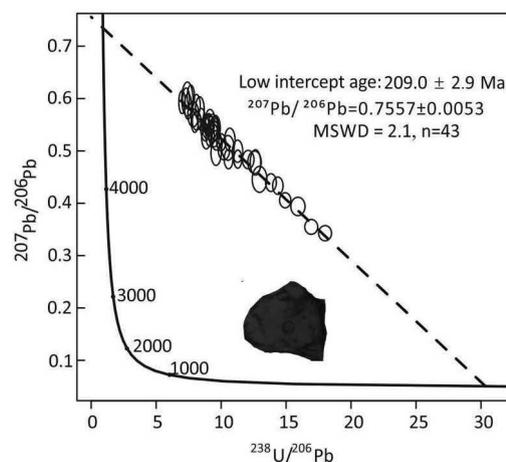

Fig. 6. Tera-Wasserburg concordia diagram of titanite from Huayangchuan deposit.

Table 1
LA-ICP-MS U-Pb isotope data of titanite from the Huayangchuan deposit.

Sample number	Pb	Th	U	Measured isotopic ratios					
		ppm		^{207}Pb/^{206}Pb	1σ	^{207}Pb/^{235}U	1σ	^{206}Pb/^{238}U	1σ
372-1	24.8250	53.1449	71.6822	0.5545	0.0137	8.4831	0.1850	0.1128	0.0017
372-2	30.4273	67.0694	113.6335	0.4885	0.0107	6.3144	0.1286	0.0946	0.0012
372-4	23.0560	54.1394	85.9164	0.5330	0.0152	6.7352	0.1554	0.0937	0.0014
372-5	27.2029	47.6945	62.6366	0.6110	0.0149	11.3369	0.2309	0.1370	0.0021
372-6	90.7100	48.3244	62.9305	0.5516	0.0162	7.9174	0.1777	0.1073	0.0019
372-7	39.2995	76.6698	202.9967	0.4410	0.0090	4.7406	0.1373	0.0772	0.0014
372-8	37.7604	93.1837	231.8909	0.4077	0.0081	3.7445	0.0703	0.0670	0.0008
372-9	35.6732	86.3409	196.1508	0.4415	0.0091	4.3773	0.0872	0.0723	0.0009
372-11	25.6681	55.1387	82.1527	0.5487	0.0137	7.8917	0.1782	0.1055	0.0016
372-12	22.0133	57.5226	67.1262	0.5712	0.0149	8.4319	0.1812	0.1094	0.0017
372-14	21.2605	41.1355	69.0416	0.5551	0.0160	7.8306	0.1846	0.1045	0.0016
372-15	47.1608	112.7869	403.2729	0.3434	0.0070	2.6245	0.0543	0.0556	0.0006
372-16	22.5882	47.0965	64.2509	0.5647	0.0125	9.0990	0.1920	0.1179	0.0017
372-17	27.4717	157.0607	182.5139	0.3967	0.0094	3.4120	0.0787	0.0628	0.0009
372-18	26.2758	56.5303	70.1312	0.5646	0.0137	9.6405	0.2098	0.1254	0.0018
372-19	32.6287	192.5679	244.0397	0.3580	0.0080	2.8876	0.0586	0.0590	0.0007
372-20	34.9878	97.6329	198.3242	0.4353	0.0088	4.1583	0.0806	0.0696	0.0008
372-21	23.9968	103.5688	73.4227	0.5634	0.0145	8.3251	0.1686	0.1098	0.0018
372-22	20.9644	48.3376	64.4966	0.5342	0.0139	8.1520	0.1830	0.1129	0.0018
372-23	22.6489	49.2817	76.0417	0.5394	0.0139	7.7559	0.2036	0.1057	0.0019
372-24	18.3896	33.8335	50.7407	0.5938	0.0168	9.5579	0.2246	0.1197	0.0020
372-25	22.7705	52.1696	86.4942	0.5067	0.0109	6.7512	0.1505	0.0979	0.0017
372-26	21.1075	44.4631	63.9282	0.5620	0.0145	8.3831	0.1880	0.1106	0.0018
372-27	29.5072	92.9353	64.6779	0.5980	0.0124	11.6967	0.2429	0.1431	0.0020
372-28	22.8970	64.5567	102.6896	0.4897	0.0108	5.5147	0.1172	0.0828	0.0013
372-29	20.0610	46.4010	77.9229	0.5135	0.0137	6.6225	0.1762	0.0950	0.0018
372-30	23.0535	63.2425	59.9586	0.5963	0.0131	9.9978	0.2040	0.1235	0.0018
372-31	22.0633	41.1258	66.4820	0.5557	0.0160	8.4934	0.2007	0.1138	0.0019
372-32	25.6539	53.1231	93.3471	0.5004	0.0119	7.1097	0.1819	0.1041	0.0017
372-33	22.2013	63.5715	68.7889	0.5603	0.0153	8.0594	0.1865	0.1068	0.0017
372-34	22.7226	49.0468	69.9744	0.5400	0.0135	7.9837	0.1785	0.1093	0.0016
372-35	39.8747	120.7763	162.9961	0.4902	0.0105	5.9147	0.1089	0.0886	0.0010
372-36	14.1705	15.2301	34.0774	0.6163	0.0204	11.1547	0.3635	0.1351	0.0032
372-37	25.9538	104.9997	120.5743	0.4832	0.0129	5.2112	0.1278	0.0791	0.0010
372-39	25.5217	45.1805	61.6699	0.5925	0.0143	10.8147	0.2462	0.1342	0.0020
372-40	35.7881	63.2124	126.2008	0.5199	0.0099	7.1159	0.1365	0.1000	0.0014
372-41	23.9993	60.7770	96.9565	0.5051	0.0124	6.1074	0.1378	0.0888	0.0013
372-42	24.0819	46.3498	80.5759	0.5297	0.0131	7.4448	0.1606	0.1038	0.0016
372-43	24.0094	45.3491	59.1794	0.6119	0.0142	10.8439	0.2290	0.1304	0.0019
372-44	21.9609	60.6805	104.2876	0.4848	0.0122	5.2436	0.1308	0.0796	0.0013
372-45	23.0790	48.2669	62.1516	0.5679	0.0135	9.4668	0.2012	0.1233	0.0021
372-46	22.0754	40.7437	57.7406	0.5755	0.0139	10.0020	0.2773	0.1273	0.0028
372-48	22.2408	55.0699	67.4063	0.5651	0.0169	8.3758	0.2055	0.1106	0.0022

Table 2
Re–Os isotope data of molybdenite from Huayangchuan deposit.

| Sample	Weight (g)	Re (ppm)		^{187}Re (ppm)		^{187}Os (ppm)		Age (Ma)	
		content	2σ	content	2σ	content	2σ	model T	2σ
zk-2403Mo-1	0.0239	390.2485	3.388	245.2865	2.1295	0.811207	0.005647	198.18	2.20
zk-2403Mo-3	0.0229	392.7483	3.9707	246.8577	2.4957	0.81699	0.003306	198.33	2.16
zk-8401Mo-6	0.0136	374.8899	2.6333	235.6330	1.6551	0.768338	0.002533	195.40	1.51
zk-8401Mo-7	0.0137	337.5492	2.3657	212.1629	1.4869	0.696981	0.006351	196.86	2.26
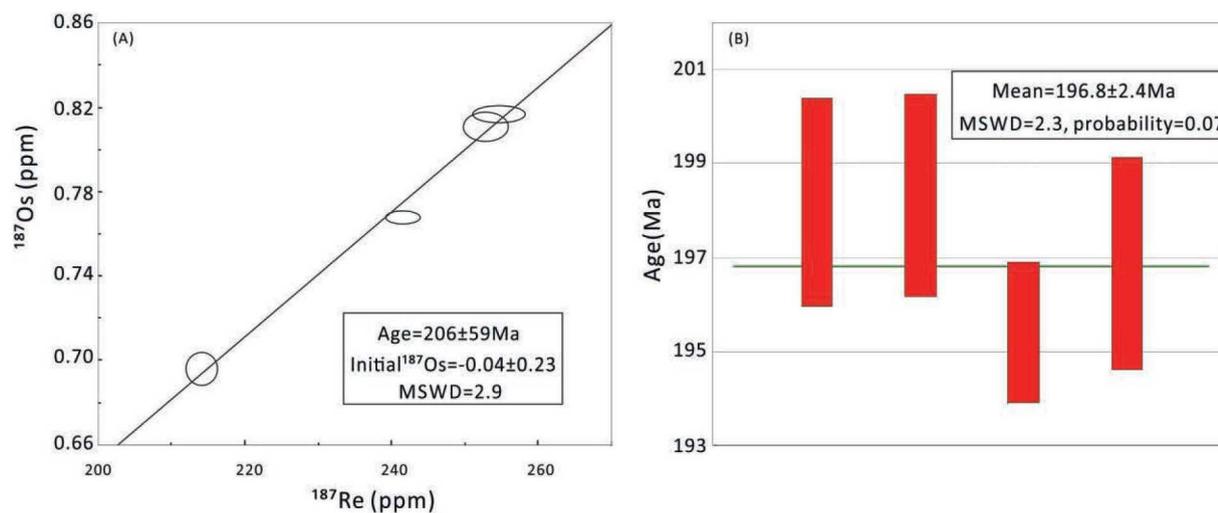
Fig. 7. (A) Molybdenite Re–Os isochron age plot. (B) Molybdenite Re–Os weighted mean modal age plot.

6. Discussion

6.1. Genesis of titanite and implications for mineralization

Elements substitution in titanite ($CaTi(SiO_4)O$) usually occurs in four sites, i.e., tetrahedral Si, octahedral Ti, sevenfold decahedral Ca and underbonded O1 site (Ribbe, 1980; Frost et al., 2000; Kohn, 2017). The Ti site is usually substituted by Al, Fe and other larger ions such as Nb, Ta, Zr and Sn. The O1 site is commonly substituted by F and Cl, whilst the substitution of Si is rare (Frost et al., 2000; Kohn, 2017). Unusual 7-fold Ca site can be substituted by large ions (such as REEs, U, Th, Mn Na, Sr and Pb; Green and Pearson, 1986; Frost et al., 2000; Kohn, 2017). The ideal composition of titanite (without substitution) comprises 28.60 wt.% CaO, 40.75 wt.% TiO_2 and 30.65 wt.% SiO_2. EPMA data of the Huayangchuan titanite (Supplementary Table 2) show distinctly lower CaO (25.19–28.41 wt.%) and TiO_2 (29.82–36.43 wt.%) than the ideal values, but the average SiO_2 content (29.65 wt.%) is similar. In additional, significant contents of Nb, Fe, Al, REE (Ce and Nd), Na and F were detected. It is thus clear that titanite in the Huayangchuan carbonatite experienced complex substitutions (Fig. 8A–C), which may have taken place via the following three reactions (Ribbe, 1980; Green and Pearson, 1986; Kohn, 2017; Pan et al., 2018).

The highly negative Ti vs. (Nb + Fe + Al) correlation (Fig. 8A) in titanite may have led by the following substitution reaction:

$$2Ti^{4+} = (Nb, Ta)^{5+} + (Al, Fe)^{3+} \tag{1}$$

The negative (Ti + Ca) vs. (Fe + Al + REE) correlation (Fig. 8B) may have led by the following substitution reaction:

$$Ca^{2+} + Ti^{4+} = REE^{3+} + (Al, Fe)^{3+} \tag{2}$$

The weakly negative (Fe + Al) vs. F correlation (Fig. 8C) may have led by the following substitution reaction:

$$Ti^{4+} + O^{2-} = (Al, Fe)^{3+} + (F, OH)^{-} \tag{3}$$
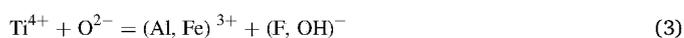
Element substitutions in minerals usually reflect geochemical characteristics. Firstly, Nb^{5+} (0.64 Å), Ta^{5+} (0.64 Å), Fe^{3+} (0.65 Å) and Al^{3+} (0.54 Å) have similar ionic radius with Ti^{5+} (0.61 Å) at VI co-ordination site, while REE^{3+} (La – Y: 1.10–0.96 Å) at VII co-ordination site also has similar ionic radius with Ca^{2+} (1.08 Å). Thus, reactions (1) and (3) substitution in titanite can easily occur when the melt or fluid are rich in these elements. Secondly, the analyzed titanite in Huayangchuan carbonatite closely coexists with pyrochlore (main Nb-bearing ore mineral in Huayangchuan deposit), and Nb is a characteristic trace element of carbonatite (Woolley and Kempe, 1989), which could enhance the reaction (1) substitution during titanite crystallization and Nb mineralization at Huayangchuan. In addition, carbonatite commonly has abundant REE comparing with other igneous rocks (Woolley and Kempe, 1989), which can strengthen the reaction (2) substitution through REE replacing Ca in titanite.

The substitution reactions (1) to (3) show a strong to weak correlation trend (Fig. 8), indicating that the major economic element (e.g., Nb) is closely related to the titanite crystallization at Huayangchuan.

6.2. Timing of the Huayangchuan U-polymetallic mineralization

The alkali-U ore-related titanite at Huayangchuan yielded a ^{206}Pb/^{238}U age of 209.0 ± 2.9 Ma, which is coeval with the published ore-related feldspar K–Ar age (206 Ma) and carbonatite K–Ar age (204 Ma; Qiu et al., 1993). This provides direct geochronological evidence for a Late Triassic carbonatite U-polymetallic mineralization event at Huayangchuan, and implies that the younger ages reported likely represent a post-mineralization thermal event, e.g., hydrothermal biotite Ar–Ar age: 132.58 ± 0.70 Ma (He et al., 2016). This biotite formed after carbonatite invaded the host rock, thus this biotite Ar–Ar age doesn't represent simultaneous carbonatite product. The younger Cretaceous (late Yanshanian) thermal event may have caused by the Yanshanian Huashan and Laoniushan granites located in the north and south of Huayangchuan, respectively (Fig. 2A).
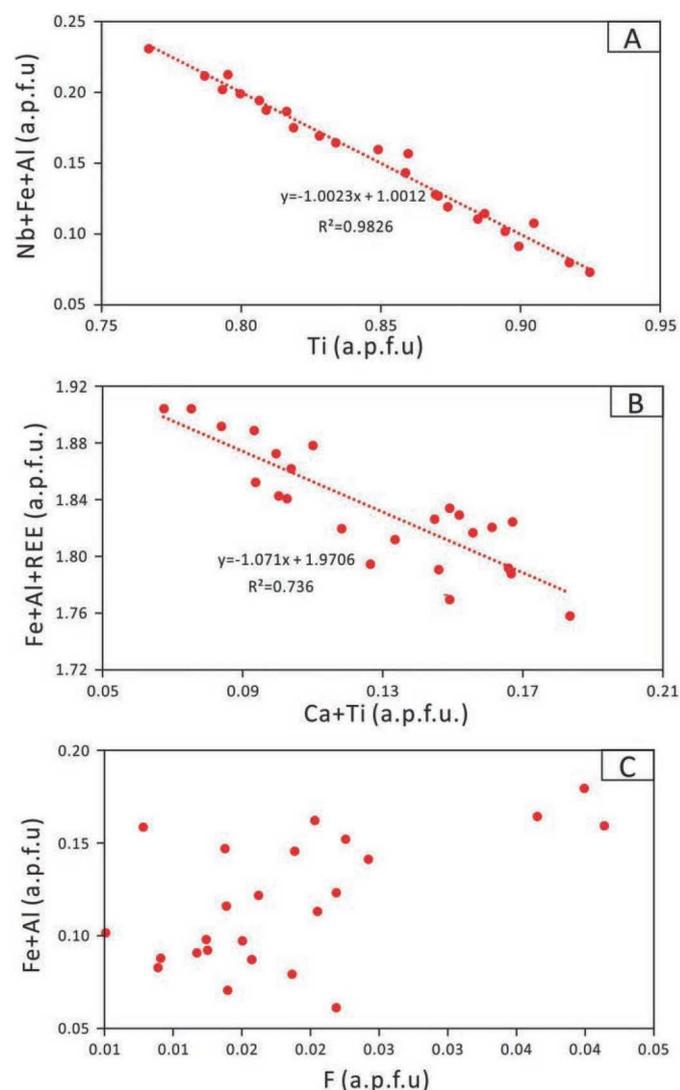
Fig. 8. Relationship of elemental substitution in titanite. (A) Ti vs. (Nb + Fe + Al). (B) (Ca + Ti) vs. (Fe + Al + REE). (C) F vs. (Fe + Al).

The molybdenite grains we dated were from the late main ore stage (Fig. 5A, B), in the mineral assemblage of pyrochlore + monazite + allanite + calcite + phlogopite ± biotite. Thus, the weighted mean age of 196.8 ± 2.4 Ma can represent the lower limit of the main ore stage at Huayangchuan.

6.3. Implications for carbonatite origin and Triassic metallogeny in Qinling Orogen

Rhenium is a siderophile element, which is commonly more enriched in the mantle and mafic-ultramafic rocks. Thus, the molybdenite Re contents of mantle-derived ores are generally higher than those from the crust (Mao et al., 1999; Stein et al., 2001). Mao et al. (1999) suggested that the molybdenite Re contents of ores increase from a crust source (ppm-scale), through crust-mantle mixed source (tens of ppm), to mantle source (hundreds of ppm). Molybdenite grains from the Huayangchuan carbonatite contain 337.55–392.75 ppm Re, reflecting possibly a mantle-derived ore-material source, similar to the Huanglongpu carbonatite-hosted Mo-Pb(-Re) deposit (molybdenite Re content: 159.40–633.10 ppm, $n = 13$; Huang et al., 1994; Stein et al., 1997; Deng et al., 2009) and Huangshuian carbonatite-hosted Mo(-Pb) deposit (molybdenite Re content: 60.12–154.50 ppm, $n = 11$; Huang et al., 2009; Cao et al., 2014) in the region. In addition, the $\delta^{13}C$ (−6.6‰ to −7.0‰),

$\delta^{18}O$ (7.6‰–8.4‰), $^{87}Sr/^{86}Sr$ (704,890–0.705820), $^{143}Nd/^{144}Nd$ (0.510902–0.512472), $^{206}Pb/^{204}Pb$ (17.505–18.588), $^{207}Pb/^{204}Pb$ (15.484–15.589) and $^{208}Pb/^{204}Pb$ (37.649–38.041) ratios of the Huayangchuan carbonatites also show mantle-derived signatures (Xu et al., 2007; Huang et al., 2009; Hui et al., 2017). From the Archean to Cenozoic, the Qinling Orogen may have experienced multi-stage tectonic process of rifting, collision and amalgamation (Zhang et al., 1996, 2001). The North Qinling terrane was separated from the South China Block and drifted northward toward the North China Block at ca. 800 Ma (Wu and Zheng, 2013). In the Paleozoic, the Erlangping backarc basin was likely formed by the north-dipping subduction of the North Qinling. Meanwhile, the Mianlue ocean basin may have opened by the break-up of the South Qinling terrane from South China (Wu and Zheng, 2013). During the Carboniferous, the Mianlue oceanic basin may have started subducting northward to cohere with the South Qinling, leading eventually to the Triassic collision between the South China and North China Blocks (Zhang et al., 1996; Chen, 2010; Wu and Zhang, 2013).

In the Triassic, Qinling Orogen may have been affected complex tectonism and developed coeval carbonatite magmatism and related mineralization, including those at Huayangchuan, Huanglongpu and Huangshuian (Figs. 1A and 9; Table 3). The Huanglongpu carbonatite-hosted Mo-Pb(-Re) deposit shares similar geological features with the nearby (ca. 8 km distance) Huayangchuan. Molybdenite Re–Os, ilmenite U–Pb, and monazite U–Th–Pb dating of the Huanglongpu ores/ore-related rocks yielded 231–220 Ma, 206 Ma, 214–209 Ma, respectively (Huang et al., 1984, 1994, 1995; Song et al., 2016; Stein et al., 1997). Song et al. (2015) reported molybdenite Re–Os age of 225.0 ± 7.6 Ma from the Yuantou Mo deposit (also in the Huanglongpu orefield). For the Huangshuian Mo deposit, molybdenite Re–Os and bastnäsite U–Pb dating yielded similar Late Triassic ages of 210–208 Ma and 206.5 ± 3.8 Ma, respectively (Huang et al., 2009; Cao et al., 2014; Zhang et al., 2019). At the Miaoya REE-Nb deposit, whose mineralization is interpreted to be multiphase (Zhang et al., 2019), monazite and columbite U–Pb dating yielded Middle-Late Triassic ages of 243–231 Ma (Xu et al., 2014; Ying et al., 2017; Zhang et al., 2019), and the very recent bastnäsite U–Pb dating yielded a younger Late Triassic age of 205.8 ± 3.6 Ma (Zhang et al., 2019). Apart from these above-mentioned Triassic carbonatite-hosted deposits, many other types of deposits in the Qinling Orogen were also dated to be Triassic, including the Dahu quartz-vein-type Au deposit (255.6–215.4 Ma; Li et al., 2007, 2008) and quartz-vein-type Mo deposits (e.g., Qianfanling, Zhifang, Daxigou and Maogou) in the Soxian orefield (248.2–215.0 Ma; Gao et al., 2010; Gao, 2011).

The mantle origin of the Huayangchuan carbonatite has been proposed based on C-O-Sr-Nd-Pb isotopes studies (Xu et al., 2007, 2011; Huang et al., 2009; Hui et al., 2017). In addition, Mg isotopes of Huayangchuan and Huanglongpu carbonatites ($\delta^{26}Mg$: 1.07‰ to −1.28‰) reveal that mantle-originated carbonatite may partially come from recycled marine carbonate (Song et al., 2016), showing some genetic connection with subduction and resulted back arc extension (Xu et al., 2009; Chen et al., 2010). However, low-degree partial melting of metasomatized mantle can generate carbonatite with similar geochemical signatures, such tectonic processes include crust thickening and following delamination during post-collision (Song et al., 2016); extension or rifting during post-collision orogenesis of the North China Block and South China Block (Huang et al., 2009). Carbonatites in the Lower Qinling district all have similar ages, i.e., 231–209 Ma for Huanglongpu (Huang et al., 1984, 1994, 1995; Stein et al., 1997; Song et al., 2016), 210–206 Ma for Huangshuian (Huang et al., 2009; Cao et al., 2014; Zhang et al., 2019), and 206–204 Ma for Huayangchuan (Qiu et al., 1993), which are generally consistent with the Huayangchuan mineralization ages of 209–196 Ma (this study). This indicates the Late Triassic carbonatite and associated U-Nb-Mo-REE mineralization in the Lower Qinling area were generally formed in similar tectonic setting, although the detailed processes are still in debate.

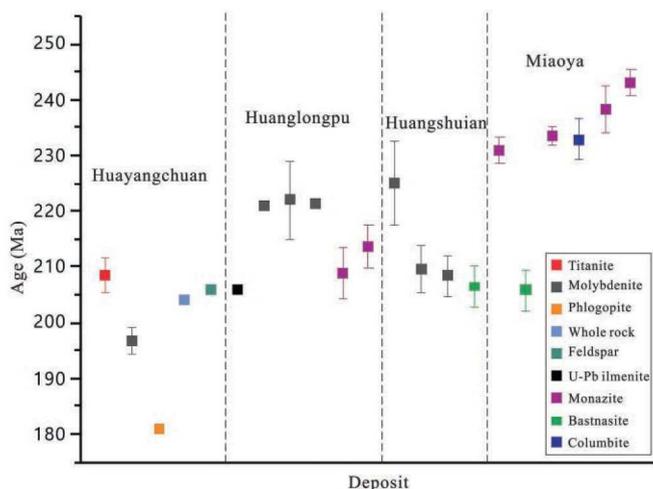Paleomagnetic study by Zhao and Coe (1987) suggested that the

Fig. 9. Summary of geochronological data for the Triassic carbonatite-hosted deposits in the Qinling Orogen. Data and references are listed in Table 3.

South China and the North China Blocks started colliding in the Permian-Triassic, with a 67° clockwise rotation for South China. This may have caused a diachronous collision from east to west in the Qinling Orogen, as supported by the older emplacement ages of carbonatites in the eastern Qinling Orogen (e.g., Miaoya). The regional tectonics may have transformed into extensional after the collision in the late Triassic,

which formed a series of NW or WNW-trending deep faults and coeval mantle-derived carbonatite magmatism in the orogen (e.g., Huayang-chuan, Huanglongpu and Huangshuian) (Huang et al., 2009). Meanwhile, crustal-sourced fluids may have led to the formation of the Dahu and Soxian quartz-vein deposits along brittle-ductile shear zones (Li et al., 2007; Gao et al., 2010, 2011). However, Re contents in Molybdenite of Dahu and Soxian quart-vein deposit are 215.4–255.6 ppm ($N = 9$; Li et al., 2007; Li et al., 2008) and 215–248.2 ppm ($N = 17$; Gao et al., 2010; Gao, 2011), respectively, much higher than common deposits deriving from crust source, which usually contain only several ppm Re in molybdenite (Mao et al., 1999), indicating a similar mantle component may also have involved into the ore-forming process. After the Triassic, the Jurassic-Cretaceous (Yanshanian) magmatism and associated mineralization occurred extensively in the Qinling Orogen due to the tectonic transform at the east of China, including porphyry/porphyry-related skarn-type Mo-W-Cu deposits in the southern margin of the North China Block, e.g., Jinduicheng porphyry Mo deposit (139 ± 3.0 Ma; Huang et al., 1994), Donggou porphyry Mo deposit (116 Ma; Ye et al., 2006), Nannihu porphyry-skarn Mo(-W) deposit (156–146 Ma; Huang et al., 1994) and Leimenggou porphyry Mo deposit (131 Ma; Li et al., 2006). The Yanshanian granitic magmatic and mineralization features are distinctly different from those of the Triassic carbonatite-hosted U-Mo-REE polymetallic deposits in the orogen. The Huayangchuan supergiant U-polymetallic ore formation (209–196 Ma) suggest significant Triassic carbonatite-related mineralization in the Qinling Orogen, especially in the southern margin of the North China Block.

Table 3
Age and geological summary of the Triassic carbonatite deposits in the Qinling Orogen.

Deposit	Resource	Scale	Host rock	Sample	Methods	Ages (Ma)	Reference
Huayangchuan	U (0.016%); Se (0.009%, 5826t); Sr (4%, 28.5 Mt); REE (0.085%, 0.55 Mt); Nb (0.018%, 0.11 Mt); Ba (3.8%, 27.1 Mt); Pb (0.07%, 2.2 Mt); Ag (0.0006%, 4310 t); Bi (0.009%, 62,596 t)	Supergiant	Carbonatite Ores	Titanite	LA-ICP-MS U–Pb	208.5 ± 3.2	This study
			Carbonatite	Molybdenite	ICP-MS Re–Os	196.8 ± 2.4	This study
			Carbonatite	Phlogopite	K–Ar	181	Yu (1992)
			Carbonatite	Whole rock	K–Ar	204	Qiu et al. (1993)
			Carbonatite	Feldspar	K–Ar	206	
Huanglongpu	Mo (0.086%, 0.12 Mt); Pb (0.19 Mt)	Large	Carbonatite Ores	Uranium-lead ilmenite	U–Th–Pb	206	Huang et al. (1984)
			Carbonatite	Molybdenite	Re–Os	221	Huang et al. (1994)
			Carbonatite	Molybdenite	Re–Os	222 ± 7	Huang et al. (1995)
			Carbonatite	Molybdenite	Re–Os	221.5 ± 0.3	Stein (1997)
			Carbonatite	Monazite	SIMS U–Pb	208.9 ± 4.6	Song et al. (2016)
			Carbonatite	Monazite	SIMS Th–Pb	213.6 ± 4.0	
			Carbonatite	Molybdenite	ICP-MS Re–Os	225.0 ± 7.6	Song et al. (2015)
Huangshuian	Mo (0.082%, 0.20 Mt)	Large	Carbonatite	Molybdenite	ICP-MS Re–Os	209.5 ± 4.2	Huang et al. (2009)
			Carbonatite	Molybdenite	ICP-MS Re–Os	208.4 ± 3.6	Cao et al. (2014)
			Carbonatite	Bastnaesite	LA-ICP-MS Th–Pb	206.5 ± 3.8	Zhang et al. (2019)
Miaoya	Nb (0.1%, 0.93 Mt); REE (1.55%, 1.22 Mt)	Large	Carbonatite	Monazite	LA-ICP-MS U–Pb	231.0 ± 2.3	Zhang et al. (2019)
			Carbonatite	Bastnaesite	LA-ICP-MS U–Pb	205.8 ± 3.6	
			Carbonatite	Monazite	SHRIMP U–Pb	233.6 ± 1.7	Xu et al. (2014)
			Carbonatite	Columbite	LA-ICP-MS U–Pb	232.8 ± 3.7	Ying et al. (2017)
			Carbonatite	Monazite	LA-ICP-MS U–Pb	238.3 ± 4.1	
			Syenite	Monazite	LA-ICP-MS U–Pb	243.1 ± 2.5	

7. Conclusions

(1) Ore-related titanite grains from the Huayangchuan carbonatite are enriched in HFSEs, and show clear elemental substitutions with weakly positive Ce anomalies.

(2) The high molybdenite Re contents (337.55–392.75 ppm) implies a mantle origin for the ore-forming materials and thus the ore-hosting carbonatites. This conclusion is consistent with the C-O-Sr-Nd-Pb isotope evidence.

(3) The main-ore stage titanite yielded a $^{206}Pb/^{238}U$ age of 209.0 ± 2.5 Ma. This Late Triassic carbonatite-related mineralization at Huayangchuan is coeval with the closure of the Mianlue ocean. The molybdenite from the late main-ore stage yielded a weighted mean Re–Os age of 196.8 ± 2.4 Ma, which constrained the lower age limit of the Huayangchuan carbonatite mineralization.

Declaration of competing interest

The authors declare that they have no known competing financial interests or personal relationships that could have appeared to influence the work reported in this paper.

Acknowledgments

Appendix A. Supplementary data

Supplementary data to this article can be found online at https://doi.org/10.1016/j.gsf.2020.03.001.

References

Aleinikoff, J.N., Wintsch, R.P., Fanning, C.M., Dorais, M.J., 2002. U–Pb geochronology of zircon and polygenetic titanite from the Glastonbury Complex, Connecticut, USA: an integrated SEM, EMPA, TIMS, and SHRIMP study. Chem. Geol. 188, 125–147.

Andersen, T., 2002. Correction of common lead in U–Pb analyses that do not report ^{204}Pb. Chem. Geol. 192, 59–79.

Cao, J., Ye, H.S., Li, H.Y., Li, Z.Y., Zhang, X.K., He, W., Li, C., 2014. Geological characteristic and molybdenite Re-Os isotopic dating of Huangshuian carbonatite vein-type Mo (Pb) deposit in Songxian County, Henan Province. Miner. Deposits 33, 53–69 (in Chinese with English abstract).

Chen, Y.J., 2010. Indosinian tectonic setting, magmatism and metallogenesis in Qinling Orogen, central China. Chin. Geol. 37, 854–865 (in Chinese with English abstract).

Cherniak, D., 1993. Lead diffusion in titanite and preliminary results on the effects of radiation damage on Pb transport. Chem. Geol. 110, 177–194.

Chew, D.M., Petrus, J.A., Kamber, B.S., 2014. U–Pb LA–ICPMS dating using accessory mineral standards with variable common Pb. Chem. Geol. 363, 185–199.

Dahlkamp, F.J., 1993. Uranium Ore Deposits. Springer, Berlin Heidelberg, 1-460.

Deng, X.H., Yao, J.M., Li, J., Sun, Y.L., 2009. Molybdenite Re-Os isotope age of Zhaiwa Mo deposit and implications for Xionger mineralization in eastern Qinling Orogen. Acta Petrol. Sin. 25, 2739–2746 (in Chinese with English abstract).

Frost, B.R., Chamberlain, K.R., Schumacher, J.C., 2000. Sphene (titanite): phase relations and role as a geochronometer. Chem. Geol. 172, 131–148.

Fu, Y., Sun, X., Zhou, H., Lin, H., Yang, T., 2016. In-situ LA–ICP–MS U–Pb geochronology and trace elements analysis of polygenetic titanite from the giant Beiya gold–polymetallic deposit in Yunnan Province, Southwest China. Ore Geol. Rev. 77, 43–56.

Gao, C., Kang, Q.Q., Jiang, H.J., Zheng, H., Li, P., Zhang, X.M., Li, L., Dong, Q.Q., Ye, X.C., Hu, X.J., 2017. A unique uranium polymetallic deposit discovered in the Qinling orogenic belt: the Huayangchuan super-large U-Nb-Pb-REE deposit associated with pegmatites and carbonatites. Geochemistry 46, 449–455 (in Chinese with English abstract).

Gao, X.Y., Zheng, Y.F., Chen, Y.X., Guo, J., 2012. Geochemical and U–Pb age constraints on the occurrence of polygenetic titanites in UHP metagranite in the Dabie orogen. Lithos 136–139, 93–108.

Gao, Y., Li, Y.F., Guo, B.J., Cheng, G.X., Liu, Y.W., 2010. Geological characteristic and molybdenite Re-Os isotopic dating of Qianfangling quartz-vein Mo deposit in

Songxian country, western Henan Province. Acta Petrol. Sin. 26, 757-757 (in Chinese with English abstract).

Gao, Y., 2011. Geology, Geochemistry and Genesis of Qianfangling Quartz-Vein Mo Deposit in Songxian Country Western Henan Province, Ph.D. thesis. China University of Geosciences, Beijing (in Chinese).

Glorie, S., Jepson, G., Konopelko, D., Mirkamalov, R., Meeuws, F., Gilbert, S., Gillespie, J., Collins, A.S., Xiao, W., Dewaele, S., De Grave, J., 2019. Thermochronological and geochemical footprints of post-orogenic fluid alteration recorded in apatite: implications for mineralisation in the Uzbek Tian Shan. Gondwana Res. 71, 1–15.

Green, T.H., Pearson, N.J., 1986. Rare-earth element partitioning between sphene and coexisting silicate liquid at high pressure and temperature. Chem. Geol. 55, 105–119.

Huang, D.H., Wang, Y.C., Nie, F.J., Jiang, X.J., 1984. Isotopic composition of sulfur, carbon and oxygen and source material of the Huanglongpu carbonatite vein-type of molybdenum(lead) deposits. Acta Geol. Sin. 58, 252–264 (in Chinese with English abstract).

Huang, D.H., Wang, C.Y., Nie, F.J., Jiang, X.J., 1985. A new type of molybdenite deposit—geological characteristic and metallogenic mechanism of the Huanglongpu carbonatite vein-type of molybdenite (lead) deposit, Shaanxi. Acta Geol. Sin. 3, 61–95 (in Chinese with English abstract).

Huang, D.H., Wu, C.Y., Du, A.D., He, H.L., 1994. Re-Os isotope ages of molybdenite deposits in east Qinling and their significance. Miner. Deposits 13, 221–230 (in Chinese with English abstract).

Huang, D.H., Wu, C.Y., Du, A.D., He, H.L., 1995. Re-Os Isotope ages of molybdenum deposits in East Qinling and their significance. Chin. J. Geochem. 14, 313–322.

Huang, D.H., Hou, Z.Q., Yang, Z.M., Li, Z.Q., Xu, D.X., 2009. Geological and geochemical characteristics, metallogenic mechanism and tectonic setting of carbonatite vein-type Mo (Pb) deposits in the East Qinling molybdenum ore belt. Acta Geol. Sin. 83, 1968–1984 (in Chinese with English abstract).

He, S., Li, Z.Y., Hui, X.C., Guo, J., 2016. $^{40}Ar/^{39}Ar$ geochronology of biotite in Huayangchuan uranium-polymetallic deposit in Shaanxi province and its geological significance. Uran. Geol. 32, 159–164 (in Chinese with English abstract).

He, S., Hui, X.C., Guo, J., 2018. U-Nb-REE mineralization characteristics of Huayangchuan uranium polymetallic deposit, Shaanxi province. World Nuclear Geosci. 4, 203–209 (in Chinese with English abstract).

Hui, X.C., He, S., 2016. Mineralization characteristic of carbonatite veins in Huayangchuan U-polymetal deposit, Shaanxi province. Uranium Geol. 32, 93–98 (in Chinese with English abstract).

Hui, X.C., Cai, Y.Q., He, S., Feng, Z.S., 2017. Petrologic and geochemical characteristics of carbonatites in Huayangchuan U-Nb-Pb deposit, Shaanxi province. Geosci. 31, 246–257 (in Chinese with English abstract).

Jiao, J.G., Tang, Z.L., Qian, Z.Z., Yuan, H.C., Yan, H.Q., Sun, T., Xu, G., Li, X.D., 2010. Metallogenic mechanism, magma source and zircon U-Pb age of Jinduicheng granitic porphyry, East Qinling. Earth Sci. 35, 1011–1022 (in Chinese with English abstract).

Jones, A.P., Genge, M., Carmody, L., 2013. Carbonate melts and carbonatites. Rev. Mineral. Geochem. 75, 289–322.

Kang, Q.Q., Jiang, H.J., Li, P., Li, L., Zhang, X.M., Dong, Q.Q., Ye, X.C., Gao, C., Zheng, T., Xue, C.C., 2018. Ore mineralogical characteristics of the Huayangchuan U-Nb-Pb deposit. J. East China Univ. Technol. 41, 111–123 (in Chinese with English abstract).

Kenedy, A.K., Kamo, S.L., Nasdala, L., Timms, N.E., 2010. Grenville skarn titanite: potential reference material for SIMS U-Th-Pb analysis. Can. Mineral. 48, 1423–1443.

King, P.L., Sham, T.-K., Gordon, R.A., Dyar, M.D., 2013. Microbeam X-ray analysis of Ce^{3+}/Ce^{4+} in Ti-rich minerals: a case study with titanite (sphene) with implications for multivalent trace element substitution in minerals. Am. Mineral. 98, 110–119.

Kirkland, C.L., Fougerouse, D., Reddy, S.M., Hollis, J., Saxey, D.W., 2018. Assessing the mechanisms of common Pb incorporation into titanite. Chem. Geol. 483, 558–566.

Kohn, M.J., 2017. Titanite petrochronology. Rev. Mineral. Geochem. 83, 419–441.

Le Bas, M., 1981. Carbonatite magmas. Mineral. Mag. 44, 133–140.

Le Bas, M.J., Kellere, J., Tao, K., Wall, F., William, C.T., Zhang, P., 1992. Carbonatite dykes at Bayan Obo, inner Mongolia, China. Mineral. Petrol. 46, 195–228.

Leng, C.B., Zhang, X.C., Hu, R.Z., Wang, S.X., Zhong, H., Wang, W.Q., Bi, X.W., 2012. Zircon U–Pb and molybdenite Re-Os geochronology and Sr–Nd–Pb–Hf isotopic constraints on the genesis of the Xuejiping porphyry copper deposit in Zhongdian, Northwest Yunnan, China. J. Asian Earth Sci. 60, 31–48.

Li, D.F., Tan, C.Y., Miao, F.Y., Liu, Q.F., Zhang, Y., Sun, X.M., 2019. Initiation of Zn-Pb mineralization in the Pingbao Pb-Zn skarn district, South China: constraints from U-Pb dating of grossular-rich garnet. Ore Geol. Rev. 107, 587–599.

Li, H.M., Ye, H.S., Mao, J.W., Wang, D.H., Chen, Y.C., Qu, W.J., Du, A.D., 2007. Re-Os dating of molybdenites from Au (-Mo) deposits in Xiaoqinling gold ore district and its geological significance. Miner. Deposits 26, 417–424 (in Chinese with English abstract).

Li, J.W., Deng, X.D., Zhou, M.F., Liu, Y.S., Zhao, X.F., Guo, J.L., 2010. Laser ablation ICP-MS titanite U–Th–Pb dating of hydrothermal ore deposits: a case study of the Tonglushan Cu–Fe–Au skarn deposit, SE Hubei Province. China. Chem. Geol. 270, 56–67.

Li, N., Sun, Y.L., Li, J., Xue, L.W., 2008. Molybdenites Re-Os isotope age of the Dahu Au-Mo deposit, Xiaoqinling and the Indosinian mineralization. Acta Petrol. Sin. 24, 810–816 (in Chinese with English abstract).

Li, Y.F., Wang, C.Q., Bai, F.J., Song, Y.L., 2004. Re-Os isotopic ages of Mo deposit in east Qinling and their geodynamic settings. Miner. Resour. Geol. 6, 571–578 (in Chinese with English abstract).

Li, N., Chen, Y.J., Santosh, M, Yao, J.M, Sun, Y.I., Li, J., 2011. The 1.85 Ga Mo mineralization in the Xiong'er Terrane, China: Implications for metallogeny associated with assembly of the Columbia supercontinent. Precambrian Res. 186, 220–232.

Li, Y.F., Mao, J.W., Liu, D.Y., Wang, Y.B., Wang, Z.L., Wang, Y.T., Li, X.F., Zhang, Z.H., Guo, B.J., 2006. SHRIMP zircon U-Pb and molybdenite Re-Os dating for the

Leimengou porphyry Mo deposit, in western Henan and its geological implication. Geol. Rev. 52, 122–131 (in Chinese with English abstract).

Liu, Y.S., Gao, S., Hu, Z.C., Gao, C.G., Zong, K.Q., Wang, D.B., 2010. Continental and oceaniccrust recycling-induced melt-peridotite interactions in the Trans-North China orogen: U–Pb dating, Hf isotopes and trace elements in zircons from mantle xenoliths. J. Petrol 51, 537–571.

Ludwig, K.R., 2003. User's Manual for Isoplot 3.00: a Geochronological Toolkit for Microsoft Excel, vol. 4. Berkeley Geochronology Centre Special Publication, pp. 1–71.

Mao, J., Zhang, Z., Zhang, Z., Du, A., 1999. Re-Os isotopic dating of molybdenites in the Xiaoliugou W (Mo) deposit in the northern Qilian mountains and its geological significance. Geochem. Cosmochim. Acta 63, 1815–1818.

Morley, C., Arboit, F., 2019. Dating the onset of motion on the Sagaing fault: evidence from detrital zircon and titanite U-Pb geochronology from the North Minwun Basin. Myanmar. Geology 47, 581–585.

Nelson, D.R., Chivas, A.R., Chappell, B.W., McCulloch, M.T., 1988. Geochemical and isotopic systematics in carbonatites and implications for the evolution of ocean-island sources. Geochem. Cosmochim. Acta 52, 1–17.

Nie, F.J., 1994. Rare earth element geochemistry of the molybdenum-bearing granitoids in the Jinduicheng-Huanglongpu district, Shaanxi Province, northwest China. Miner. Deposita 29, 488–498.

Pan, L.C., Hu, R.Z., Bi, X.W., Li, C., Wang, X.S., Zhu, J.J., 2018. Titanite major and trace element compositions as petrogenetic and metallogenic indicators of Mo ore deposits: examples from four granite plutons in the southern Yidun arc, SW China. Am. Mineral. 103, 1417–1434.

Qiu, J.X., Yu, X.H., Zeng, G.C., Li, C.N., Wang, S.J., 1993. The Alkaline Rocks of Qinling-Bashan. Geological Publishing House, Beijing, 1-183 (in Chinese).

Reguir, E.P., Chakhmouradian, A.R., Pisiak, L., Halden, N.M., Yang, P., Xu, C., Kynický, J., Couëslan, C.G., 2012. Trace-element composition and zoning in clinopyroxene- and amphibole-group minerals: implications for element partitioning and evolution of carbonatites. Lithos 128, 27–45.

Ribbe, P.H., 1980. Titanite. Rev. Mineral. Geochem. 5, 137–154.

Scibiorski, E., Kirkland, C.L., Kemp, A.I.S., Tohver, E., Evans, N.J., 2019. Trace elements in titanite: a potential tool to constrain polygenetic growth processes and timing. Chem. Geol. 509, 1–19.

Simandl, G.J., Paradis, S., 2018. Carbonatites: related ore deposits, resources, footprint, and exploration methods. B. Appl. Earth Sci. 127, 123–152.

Simonetti, A., Heaman, L.M., Chacko, T., Banerjee, N.R., 2006. In situ petrographic thin section U–Pb dating of zircon, monazite, and titanite using laser ablation–MC-ICP-MS. Int. J. Mass Spectrom. 253, 87–97.

Smith, M.P., Storey, C.D., Jeffries, T.E., Ryan, C., 2009. In situ U–Pb and trace element analysis of accessory minerals in the Kiruna district, Norrbotten, Sweden: new constraints on the timing and origin of mineralization. J. Petrol. 50, 2063–2094.

Song, S., Mao, J., Xie, G., Lei, C., Santosh, M., Chen, G., Rao, J., Ouyang, Y., 2019. In situ LA-ICP-MS U–Pb geochronology and trace element analysis of hydrothermal titanite from the giant Zhuxi W (Cu) skarn deposit, South China. Miner. Deposita 569–590.

Song, W.L., Xu, C., Qi, L., Zhou, L., Wang, L.J., Kynický, J., 2015. Genesis of Si-rich carbonatites in Huanglongpu Mo deposit, Lesser Qinling orogen, China and significance for Mo mineralization. Ore Geol. Rev. 64, 756–765.

Song, W.L., Xu, C., Smith, M.P., Kynický, J., Huang, K.J., Wei, C.W., Zhou, L., Shu, Q.H., 2016. Origin of unusual HREE-Mo-rich carbonatites in the Qinling orogen, China. Science Reports 6, 1–10.

Stacey, J.S., Kramers, J.D., 1975. Approximation of terrestrial lead isotope evolution by a two-stage model. Earth Planet Sci. Lett. 26, 207–221.

Stein, H.J., Markey, R.J., Morgan, J.W., Du, A., Sun, Y., 1997. Highly precise and accurate Re-Os ages for molybdenite from the East Qinling molybdenum belt, Shaanxi Province, China. Econ. Geol. 92, 827–835.

Stein, H.J., Markey, R.J., Morgan, J.W., Hannah, J.L., Scherstén, A., 2001. The remarkable Re-Os chronometer in molybdenite: how and why it works. Terra. Nova 13 (6), 479–486.

Storey, C.D., Jeffries, T.E., Smith, M., 2006. Common lead-corrected laser ablation ICP-MS U–Pb systematics and geochronology of titanite. Chem. Geol. 227, 37–52.

Sun, Y., Zhou, M.F., Sun, M., 2001. Routine Os analysis by isotope dilution-inductively coupled plasma mass spectrometry: OsO₄ in water solution gives high sensitivity. J. Anal. Atomic Spectrom. 16, 345–349.

Sun, Y.L., Xu, P., Li, J., He, K., Chu, Z.Y., Wang, C.Y., 2010. A practical method for determination of molybdenite Re-Os age by inductively coupled plasma-mass spectrometry combined with Carius tube-HNO₃ digestion. Analytical Methods 2, 575–581.

Sweeney, R.J., 1994. Carbonatite melt compositions in the Earth's mantle. Earth Planet Sci. Lett. 128, 259–270.

Taylor Jr., H.P., Frechen, J., Degens, E.T., 1967. Oxygen and carbon isotope studies of carbonatites from the Laacher See District, West Germany and the Alnö District, Sweden. Geochem. Cosmochim. Acta 31, 407–430.

Vermeesch, P., 2018. Isoplot R: a free and open toolbox for geochronology. Geosci. Front. 9, 1479–1493.

Wang, L.J., Xu, C., Wu, M., Song, W.L., 2011. A study of fluid inclusion from Huayangchuan carbonatite. Acta Mineral. Sin. 31, 372–379 (in Chinese with English abstract).

Wang, Y., Chen, H., Xiao, B., Han, J., Fang, J., Yang, J., Jourdan, F., 2018. Overprinting mineralization in the Paleozoic Yandong porphyry copper deposit, Eastern Tianshan, NW China—evidence from geology, fluid inclusions and geochronology. Ore Geol. Rev. 100, 148–167.

Woolley, A.R., Kempe, D.R., 1989. Carbonatites: nomenclature, average chemical compositions, and element distribution. In: Bell, K. (Ed.), Carbonatites, genesis and evolution. London, Unwin Hyman. 1–14.

Woolley, A.R., Kjarsgaard, B.A., 2008. Paragenetic types of carbonatite as indicated by the diversity and relative abundances of associated silicate rocks: evidence from a global database. Can. Mineral. 46, 741–752.

Wu, Y.B., Zheng, Y.F., 2013. Tectonic evolution of a composite collision orogen: an overview on the Qinling–Tongbai–Hong'an–Dabie–Sulu orogenic belt in central China. Gondwana Res. 23, 1402–1428.

Xu, C., Campbell, I.H., Allen, C.M., Huang, Z., Qi, L., Zhang, H., Zhang, G., 2007. Flat rare earth element patterns as an indicator of cumulate processes in the Lesser Qinling carbonatites, China. Lithos 95, 267–278.

Xu, C., Campbell, I.H., Kynicky, J., Allen, C.M., Chen, Y., Huang, Z., Qi, L., 2008. Comparison of the Daluxiang and Maoniuping carbonatitic REE deposits with Bayan Obo REE deposit, China. Lithos 106, 12–24.

Xu, C., Song, W.L., Qi, L., Wang, L.J., 2009. Geochemical characteristics and tectonic setting of ore-bearing carbonatites in Huanglongpu ore field. Acta Petrol. Sin. 25, 422–430 (in Chinese with English abstract).

Xu, C., Taylor, R.N., Kynicky, J., Chakhmouradian, A.R., Song, W., Wang, L.J., 2011. The origin of enriched mantle beneath North China block: evidence from young carbonatites. Lithos 127, 1–9.

Xu, C., Chakhmouradian, A.R., Taylor, R.N., Kynicky, J., Li, W., Song, W., Fletcher, I.R., 2014. Origin of carbonatites in the south Qinling orogen: implications for crustal recycling and timing of collision between the South and North China Blocks. Geochem. Cosmochim. Acta 143, 189–206.

Ye, H.S., Mao, J.W., Li, Y.F., Guo, B.J., Zhang, C.Q., Liu, J., Yan, Q.R., Liu, G.Y., 2006. SHRIMP zircon U-Pb and molybdenite Re-Os dating for the supergiant Donggou porphyry Mo deposit in east Qinling, China and its geological implication. Acta Geol. Sin. 80, 1079–1088 (in Chinese with English abstract).

Ying, Y., Chen, W., Lu, J., Jiang, S.-Y., Yang, Y., 2017. In situ U–Th–Pb ages of the Miaoya carbonatite complex in the South Qinling orogenic belt, central China. Lithos 290, 159–171.

Yu, X.H., 1992. Geological, mineralogical characteristics and origin of the carbonatites from Huayangchuan, Shaanxi Province. Earth Sci. 17, 151–158 (in Chinese with English abstract).

Zack, T., Stockli, D.F., Luvizotto, G.L., Barth, M.G., Belousova, E., Wolfe, M.R., Hinton, R.W., 2011. In situ U-Pb rutile dating by LA-ICP-MS: [208]Pb correction and prospects for geological applications. Contrib. Mineral. Petrol. 162, 515–530.

Zhang, G.W., Meng, Q.R., Yu, Z.P., Sun, Y., Zhou, D.W., Guo, A.L., 1996. Orogenic processes and dynamics of the Qinling. Science in Chinese 26, 193–200 (in Chinese with English abstract).

Zhang, G.W., Zhang, B.R., Yuan, X.C., Xiao, Q.H., 2001. Qinling Orogenic Belt and Continental Dynamics. Science Press, Beijing, 1–855 (in Chinese with English abstract).

Zhang, W., Chen, W.T., Gao, J.F., Chen, H.K., Li, J.H., 2019. Two episodes of REE mineralization in the Qinling Orogenic Belt, Central China: in-situ U-Th-Pb dating of bastnäsite and monazite. Miner. Deposita 54, 1265–1280.

Zhao, X., Coe, R.S., 1987. Palaeomagnetic constraints on the collision and rotation of North and South China. Nature 327, 141.

Zhu, Q.Q., Xie, G.Q., Jiang, Z.S., Sun, J.F., Li, W., 2014. Characteristics and in situ U–Pb dating of hydrothermal titanite by LA-ICPMS of the Jingshandian iron skarn deposit, Hubei Province. Acta Petrol. Sin. 30 (5), 1322–1338 (in Chinese with English abstract).